ACADEMIC PRESS

Available online at www.sciencedirect.com
SCIENCE DIRECT®

Journal of Catalysis 215 (2003) 305–316

JOURNAL OF CATALYSIS

www.elsevier.com/locate/jcat

Characterization of carbon nanotubes and carbon nanofibers prepared by catalytic decomposition of acetylene in a fluidized bed reactor

M. Pérez-Cabero,[a] I. Rodríguez-Ramos,[a] and A. Guerrero-Ruíz [b,*]

[a] *Instituto de Catálisis y Petroleoquímica, CSIC, Campus de Cantoblanco, 28049 Madrid, Spain*
[b] *Departamento de Química Inorgánica y Técnica, Facultad de Ciencias, UNED, c/senda del rey, no 9, 28040 Madrid, Spain*

Received 1 October 2002; revised 6 January 2003; accepted 6 January 2003

Abstract

This article describes the synthesis of carbon nanotubes (CNTs) and carbon nanofibers (CNFs) by the catalytic decomposition of acetylene at 973 K over several Fe/silica catalysts (sol–gel method prepared) in a fluidized bed reactor. Characterization of the catalysts and the products was performed by chemical analyses, N_2 adsorption isotherms (BET surface area), temperature-programmed reduction (TPR), CO volumetric chemisorption, X-ray diffraction (XRD), temperature-programmed oxidation (TPO), and transmission electron microscopy (TEM). An apparent relationship was found to exist between the metallic iron content of the catalysts, metal particle size distribution on the surface of the silica support, and final characteristics of the carbon products obtained. High-purity CNTs and CNFs were achieved after acid treatment of the catalytically produced carbon deposits. Difficulties in exact quantitative characterization of pure CNTs in the presence of other carbon species (CNFs, capsules of carbon, amorphous carbon, etc.) are also reported and discussed.

Keywords: Carbon nanotubes; Carbon nanofibers; Fluidized bed reactor; Acetylene decomposition; Iron catalysts

1. Introduction

In the decade since the discovery of carbon nanotubes, they have captured the attention of researchers worldwide. A significant amount of work has been done to reveal the unique structural, electrical, mechanical, electromechanical, and chemical properties of carbon nanotubes (CNTs) and to explore what might be the key applications of these novel materials [1–4]. However, the full potential of carbon nanotubes for applications will not be realized until their growth can be further optimized and controlled. Among other factors, their future use strongly depends on the development of simple, efficient, and inexpensive technologies for large-scale production.

Typically, carbon nanotubes are prepared by electric arc discharge [5], laser ablation [6], and chemical vapor deposition (CVD) of hydrocarbon gases over a catalytic material [7]. The CVD method has been reported to be the most selective in carbon nanotube formation; arc discharge and laser ablation lead to mixtures of carbon materials. In addition to the purity of the product, the CVD method allows the growth of large amounts of CNTs at lower cost because it proceeds at moderate temperatures (below 1273 K). Moreover, the control of nanotube structure can be realized by regulating the reaction parameters and catalyst composition as well as by modifying the nanomorphology of the catalysts with dispersion of metals on supports [8,9].

Fe-, Ni-, and Co-supported catalysts and hydrocarbons such as methane, ethene, acetylene, carbon monoxide, and synthesis gas (CO/H_2) were employed in the CVD synthesis of carbon nanotubes [2,3,8–18]. Supports like alumina and silica have been investigated to determine the effect of the support on the size of the metal nanoparticles and the diameter and structural characteristics of carbon nanotubes. The growth of CNTs was reported to be easier over Fe catalysts than over Co or Ni [10,13]. With iron catalysts the interaction between formed carbon and metal particles is apparently less structure sensitive than with Ni or Co. This may be related to higher carbon concentration during the steady-state growth for iron catalysts [3]. The results of Hernadi et al. [13] and Dai and co-workers [14] agree with this theoretical statement, concluding that Fe/silica catalysts presented the highest activity in the decomposition of different unsatu-

* Corresponding author.
E-mail address: aguerrero@ccia.uned.es (A. Guerrero-Ruíz).

0021-9517/03/$ – see front matter
doi:10.1016/S0021-9517(03)00026-5

rated compounds. Among all the hydrocarbon gases, acetylene was reported to have the highest reactivity over the catalysts for growing better-quality CNTs [10,13]. The sol–gel synthesis method was reported to ensure a highly homogeneous distribution of transition metal ions in the silica matrix on which the nanotubes grow outward perpendicularly and form an aligned nanotube array [9,19–21].

For large-scale production the use of a fluidized bed reactor has been proposed as an alternative to avoid obstruction of the carbon materials deposited and damage to fixed bed reactor walls [22], but this kind of reactor has rarely been reported in the bibliography on carbon nanotube formation [10–12].

The syntheses of CNTs by CVD runs by a not well-defined mechanism. A first step is assumed where the carbon source is decomposed on the active points of the catalyst, and gives carbon atoms with concomitant desorption of molecular hydrogen. Carbon is then supposed to dissolve in and diffuse through the bulk of the metal, yielding finally carbon nanofibers and the metal. This general mechanism was already proposed for carbon nanofibers by Baker et al. in the 1970s and it has been widely accepted. The inverse dependence of growth rate on particle width also proposed by Baker is consistent with a diffusion-controlled mechanism [23]. The latter authors admit the formation of carbide intermediate species to explain the thermodynamics of diffusion in the last mechanism. These carbides would decompose in carbon nanofibers and the metal [24–27]. Although the formation of these carbide intermediates species is still in doubt because it is difficult to demonstrate since they constitute an intermediate species.

For this article carbon nanotubes were synthesized by the catalytic decomposition of acetylene, over several iron catalysts in a fluidized bed reactor at 973 K. Our objective was to choose the optimal conditions, for acetylene decomposition over iron catalysts, to develop one method to obtain a high yield of CNTs for further purification and characterization. Complete characterization of the catalysts and carbon species obtained was achieved and a relationship between metal particle sizes, metal contents of the catalysts and the final characteristics of carbon nanotubes was observed. We differentiate between carbon nanotubes and carbon nanofibers (CNFs), since the former have a cylinder-like structure with a channel in the middle [3], carbon encapsulation of metal particles, and amorphous carbon.

2. Materials and methods

2.1. Synthesis of the catalysts

Several Fe/silica catalysts, containing 2.5, 5, 10, and 29 wt% Fe, were prepared by a sol–gel method. The catalyst with the largest amount of metal has been already tested for carbon nanotube synthesis in our laboratory using a pulsed or fixed bed reactor [28,29].

The iron precursor for the syntheses was $Fe(NO_3)_3{\cdot}9H_2O$, and the silica precursor was tetraethoxysilane (TEOS). Ten milliliters of TEOS were mixed with an aqueous solution of the metal salt (in the exact amount to obtain the required percentages) and 10 ml of EtOH. The mixture was magnetically stirred for 20 min, and then 0.4 ml of HCl were added. The final solution was stirred 20 min longer. The mixture was then extended in a plastic plate to air-dry for 24 h. The solid formed was dried at 383 K for 22 h to completely remove the water and the solvent, and then calcined at 723 K for 16 h in an air atmosphere. The final product was ground and sieved in particle sizes between 40 and 150 μm.

2.2. Characterization of the catalysts

Iron content (wt%) of the different catalysts was analyzed in an Atomic Emission Spectroscope (ICP, Perkin–Elmer Model 3300 DV). Surface area was calculated by the conventional BET method, from the N_2 adsorption isotherms at 77 K, determined using a Micromeritics Model ASAP 2010/TRISTAR 3000 apparatus.

Temperature-programmed reduction (TPR) experiments were carried out in a microbalance (C.I. Electronic), with a small quartz basket where several milligrams of the samples were deposited. The reduction ran in a mixture of H_2/He (1/1), at a total gas flow rate of 20 ml/min, until 723 K at approximately 5 K/min, keeping the sample at this temperature for 60 min longer.

The X-ray diffraction (XRD) patterns for fresh samples and for reduced samples at 723 K with H_2 were recorded in an X-ray diffractometer (Seifert Model XRD 3000P), using Cu-K_α radiation and a graphite monochromator.

CO chemisorption measurements were performed in a conventional volumetric system at 330 K. The volumetric data were stored and analyzed by microcomputer processing. All samples were previously reduced in H_2 (20 ml/min) for 2 h at 723 K and vacuum outgassed 12 h longer at this temperature.

2.3. Synthesis of carbon nanotubes

Carbon nanotubes were synthesized by the catalytic decomposition of acetylene, over the iron catalysts previously described, in a fluidized bed reactor at 973 K. The experimental system consisted of a 2.2-cm-i.d., 120-cm-long vertical quartz reactor. A wider head was located at the upper part of the reactor to avoid catalyst loss. The reactor was heated by an 88-cm-long electric furnace (Thermolyne 79400), equipped with a proportional, integral, and differential temperature controller. The gases entered through the lower part of the reactor, coming from three Brooks 5850TR mass flow controllers. An extra thermocouple (Thermocoax Type K) was placed in the interior of the reactor, with the aim of controlling the exact temperature of the catalytic bed.

All syntheses were carried out with 6 g of the ground and sieved catalysts, deposited on a porous quartz plate placed

at half-height of the reactor. The fluidization flow rates for the experiments were calculated by measurements, at room temperature, of pressure variations in the catalytic bed of the reactor with variation of gas flows [30]. The catalyst was fluidized initially for 20 min, at room temperature, in N_2 (flow rate 600 ml/min). Then H_2 was also introduced into a mixture of N_2/H_2 (540/60 ml/min) heating from room temperature to 723 K, with a heating ramp of 10 K/min. After 10 min longer at this temperature, the reactor was heated to 973 K at 10 K/min in N_2 (600 ml/min). Once a temperature of 723 K was achieved, acetylene was introduced into a reaction mixture of $N_2/C_2H_2/H_2$ (580/15/10 ml/min) over 60 min. After this time the reactor was cooled to room temperature in an N_2 atmosphere.

The final product was obtained as a light and electrostatic black solid and was submitted to a purification procedure to eliminate the inorganic materials. The purification method consisted of elimination of the silica support in an excess of HF at room temperature and, after filtration, an oxidant treatment in excess of HNO_3 at 343 K for 1 h in a reflux system to solubilize all the iron present. The solid was then filtered, washed with distilled water, and dried at room temperature.

2.4. Characterization of the carbon materials

The products were characterized before and after purification using a series of techniques. Temperature-programmed oxidation (TPO) experiments were carried on the microbalance described above. The combustion ran in an air atmosphere, with a gas flow rate of 20 ml/min, until 1123 K at approximately 5 K/min. Four more samples, in addition to the nanotubes synthesized here, were studied. They were two commercial carbon nanotubes, from MER Corporation (MERK) and Dynamic Enterprises Ltd. (UK), a commercial high-surface-area graphite, H (300 m^2/g) (from Lonza), and a Saran carbon (980 m^2/g), prepared by carbonization of a copolymer as described in [31].

Transmission electron microscopy (TEM) studies were carried out in a JEOL JEM-2000 FX microscope at 200 kV. The samples were prepared by ultrasonic dispersal in a butanediol solution, placed on the copper TEM grid, and evaporated. Chemical analyses of the purified samples were carried out with a microanalysis system (XEDS) installed in this microscope.

Studies by XRD analysis of these final products were also performed.

3. Results

3.1. Catalyst characterization

The results of the metal analyses and BET areas for the prepared catalysts are given in Table 1. BET areas seemed, in general, to follow a growing tendency among catalysts A, B, C, and D, even though it was not strictly followed with catalysts B and C. Catalyst D, with the largest amount of iron, had the largest surface area.

Table 1
Chemical analyses and BET surface areas for catalysts A, B, C, and D

Catalyst	wt% Fe (analyses)	S_{BET} (m^2/g)
A	2.3	185
B	4.4	281
C	8.0	255
D	28.5	425

Table 2
CO uptakes over the reduced catalysts after reduction treatment[a]

Catalyst	Reduced Fe[b] (wt%)	CO chem. (μmol/g catalyst)	D (%) (1CO/2Fe)	d (nm)
A	1.4 (60)	8	6	12.5
B	4.0 (90)	24	7	10.7
C	5.3 (65)	13	3	25.0
D	15.4 (53)	12	1	75.0

[a] Reduced iron percentages and dispersion values, D (%), calculated for catalysts A, B, C, and D.

[b] Data obtained from TPR experiments. In parentheses is the percentage of reduced iron over the total iron content in the catalysts.

TPR experiments showed that the percentage of iron reduced (see Table 2), after H_2 treatments in the microbalance, was lower than 100% for all catalysts.

The crystalline phases present in the catalysts as prepared and also after reduction in H_2 were studied by XRD. The diffractograms are shown in Fig. 1. XRD patterns of catalysts A, B, and C showed diffractograms corresponding to amorphous phases before reduction. They were reduced in H_2 at 723 K but no changes in their XRD plots were observed. Only catalyst D showed iron crystalline phases before and after reduction in H_2 at 723 K. Hematite phase, Fe_2O_3, was found in the fresh catalyst D, while in the reduced one α-Fe and magnetite, Fe_3O_4, phases appeared.

To determine the number of metallic iron surface atoms present on the catalysts, CO adsorption volumetric analyses were carried out [32]. The isotherms obtained for catalysts A, B, C, and D are shown in Fig. 2. The isotherm plot tangents showed the total amount of CO chemisorbed per gram of catalyst. No second adsorption isotherms (i.e., after outgassing at room temperature) were determined because these chemisorption isotherms were obtained at low absolute pressure, less than 7 Torr, where physisorption of CO is still low. Dispersion of metallic iron, D (%), was calculated by assuming that one CO molecule is chemisorbed on two surface metallic iron atoms. The total amount of reduced iron in the catalysts was obtained from the TPR experiments. It is supposed that on reduction the iron segregates from the silica–iron matrix, forming metallic particles on the surface. The average Fe particle size, d, was calculated from $d = 0.75/D$ (nm) [33,34]. These results are also presented in

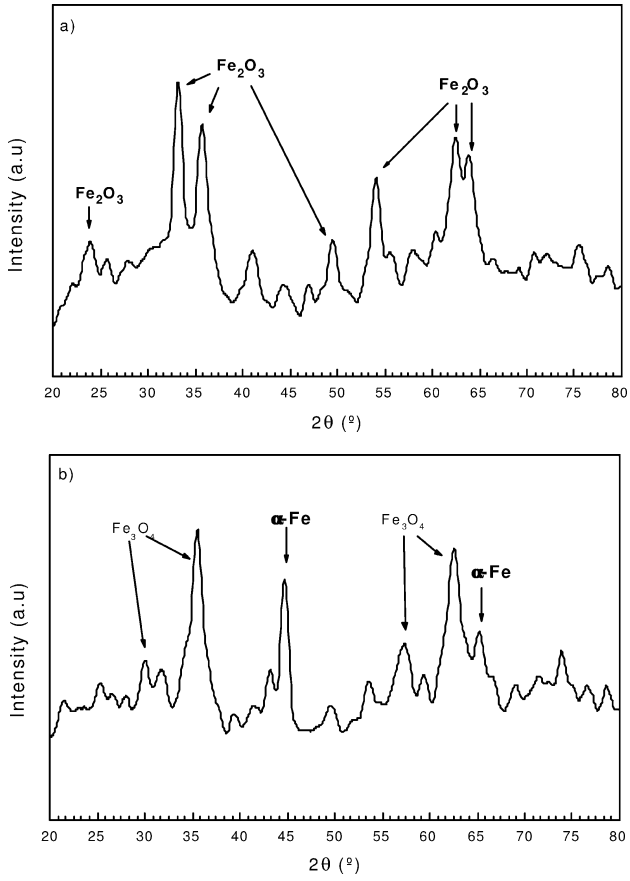

Fig. 1. XRD plots of (a) fresh catalyst D and (b) reduced catalyst D in H_2 at 450 °C.

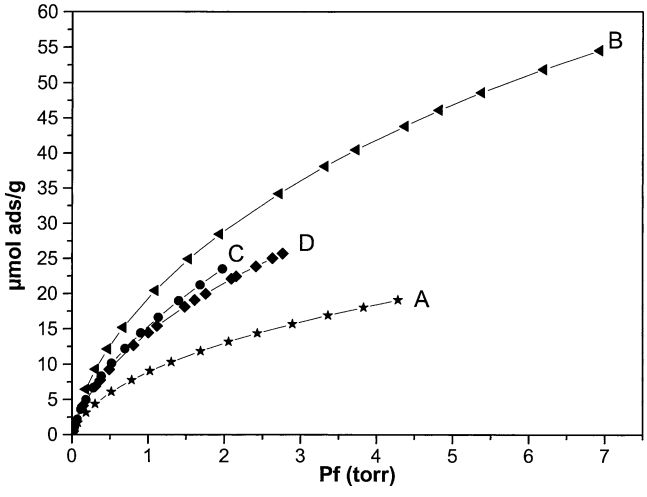

Fig. 2. CO chemisorption isotherms (330 K) for catalysts A (stars), B (triangles), C (circles), and D (squares).

Table 2. Quantitative analyses of the isotherms showed that an increment in the iron content of the catalysts resulted in a lower CO chemisorption capacity, with the exception of catalyst A.

Table 3
Thermogravimetric analyses of samples obtained from reaction with catalysts A, B, C, and D, before and after purification; two commercial CNTs (MERK and UK); Saran carbon; and H graphite

Carbon species	Reaction product (% C)	Pure product (% C)	Combustion T (K)	Final residue (wt%)
A	< 0.10	–	–	–
B	1.75	96	853	4
C	4.10	87	898	13
D	9.80	91	723/853	9
MERK	–	> 97	1023	< 3
UK	–	> 97	1073	< 3
H	–	98	963	2
Saran	–	99	833	1

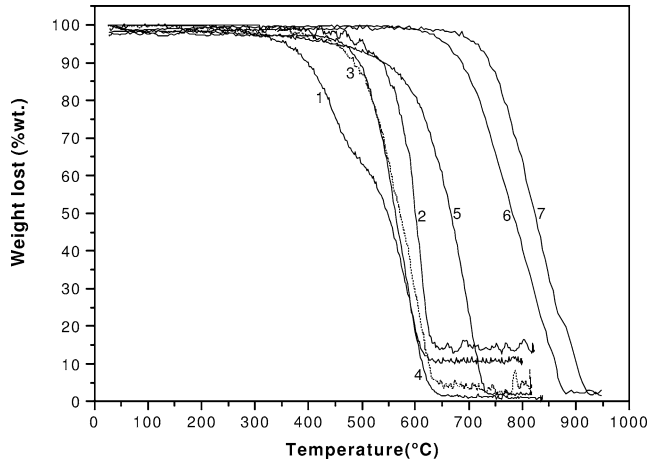

Fig. 3. Thermogravimetric analyses of purified carbon species synthesized with catalysts B (3), C (2), and D (1), commercial CNTs MERK (6) and UK (7), Saran (4), and H (5).

3.2. Product characterization

The total amount of carbon deposited on the iron–silica catalysts after reaction was determined gravimetrically by burning off the carbon materials under air flow in the thermobalance. The results in weight percent (wt%) of carbon after reaction and after purification, the combustion temperatures of both the various CNTs synthesized and the commercial products, and the final residue (in wt%) are summarized in Table 3. Catalyst A seemed to be almost inactive in the carbon formation by decomposition of acetylene. Mass losses around 0.1 wt% were observed in the thermobalance under air flow. Catalysts B, C, and D were more active and exhibited an increase in carbon deposits with higher iron content of the catalyst. Catalyst D gave carbon deposits close to 10 wt%. TPO analyses were also performed for the purified carbon products to determine their purity. Furthermore two commercial CNTs, a H graphite and a Saran carbon, were studied for comparative purposes. The thermogravimetric graphics are shown in Fig. 3. After purification the CNTs synthesized had a purity between 91 and 96 wt% carbon. The commercial products were also

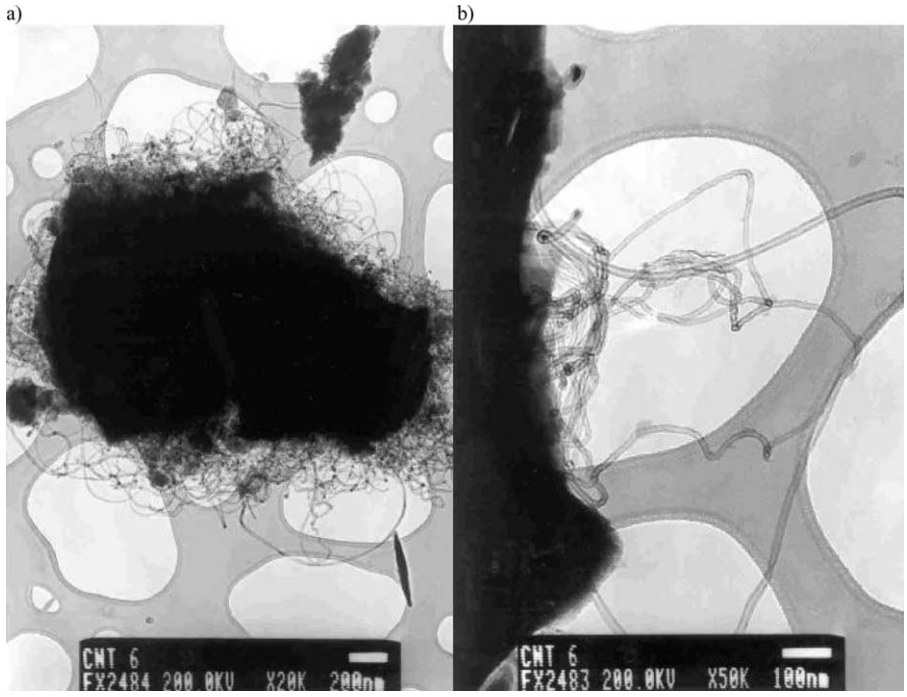

Fig. 4. TEM images of the products from reaction with catalyst A: (a) catalyst particle with CNTs growing up from the surface, (b) catalyst surface in detail.

burned with the same procedure and had a purity close to 100 wt% carbon. With these thermogravimetric profiles it is possible to establish hypotheses about the possible purity and structure of our CNTs in front of commercial products. A unique mass loss for all the carbon species was observed, except for catalyst D with two different mass losses at 723 and 853 K. CNTs B were burned at 853 K and CNTs C at 898 K. MERK and UK commercial CNTs were burned at temperatures above 1023 K, H at 963 K, and Saran at 833 K.

TEM analyses of the synthesized and purified CNTs were carried out (Figs. 4–7). TEM images revealed the presence of graphitic structures with a central channel (CNTs), structures without this central channel (CNFs and capsules of carbon), and nongraphitic structures (amorphous carbonaceous structures).

Even though catalyst A seemed to be nearly inactive for CNT synthesis, as deduced from the TPO analyses described before, TEM images showed the presence of CNTs growing from the catalyst surface (see Fig. 4). Although several long CNTs were observed in the images, their presence should be scarce and almost inappreciable in the total mass of the catalyst. CNFs, carbon encapsulation of metal particles, or amorphous carbon were not observed on this sample. Thus, this catalyst can be considered as selective for CNT formation but with very low yield in the acetylene decomposition reaction. Synthesis with catalyst B yielded large amounts of CNTs. CNFs or carbon encapsulation of metal particles were not observed. CNTs were homogeneous and most of them open at the end (see Figs. 5a and b). After purification (Figs. 5c and d), clean and homogeneous carbon nanotubes were still observed. They were narrow, 8 nm in internal diameter and 13 nm in average external diameter. All the CNTs observed were multiwalled (MWNTs). Nanotube length was not determined due to the long structures and the high density of the samples, even after purification treatments. XEDS analyses revealed the absence of iron. Also it should be noted that there were not large differences in the sizes of the CNTs before and after purification (Figs. 5a and c). This finding suggests that the CNTs remain unharmed after the purification treatment. Furthermore the nanotube walls were shown not to be completely graphitized and some defects were observed. The products from synthesis with catalyst C were mostly CNTs. TEM images for this sample are shown in Fig. 6. They had internal diameters of approximately 7–9 nm and external diameters of 8–25 nm. Some could be single-walled (SWNTs), but this was not clear in the TEM images because of the lack of resolution (Fig. 6a). Their outer walls were very deformed since large amounts of amorphous carbon were deposited on them (Figs. 6b and c). The CNTs observed were open ended and iron particles were not found. After purification (Fig. 6d) very clean CNTs were observed; however, large amounts of amorphous carbon were present in the samples. XEDS analyses revealed the absence of iron and silica. Synthesis with catalyst D gave very heterogeneous products (Fig. 7). MWNTs were observed but so were coiled structures, CNFs (Fig. 7a), lots of iron at the tips of the CNTs (Fig.7b), and carbon-encapsulated metal particles (Fig. 7c). The tubes had quite deformed walls and wide diameter distribution, approximately 8–11 nm in internal diameter and 11–25 nm in external diameter. XEDS analyses showed that the purification completely removed the silica

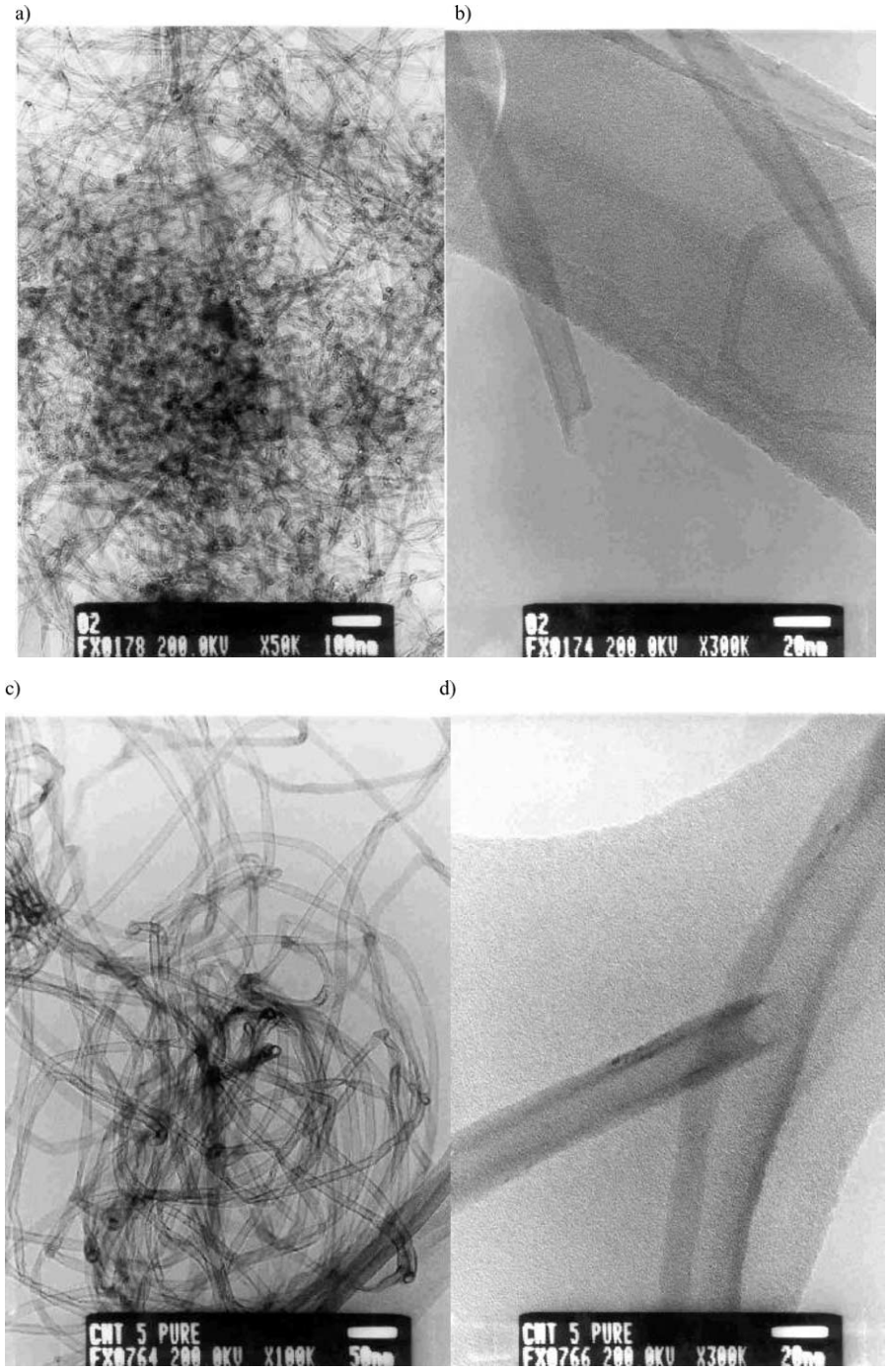

Fig. 5. TEM images of the products from reaction with catalyst B: (a) CNTs before purification treatments, (b) open nanotube end, (c) CNTs after purification treatments, (d) open nanotube end after purification treatments.

support of the catalyst even though some iron still remained. CNFs, carbon-encapsulated metal particles, large amounts of iron at CNT tips, and amorphous carbon were still present after purification (Figs. 7c and d).

XRD analyses were carried out for the samples synthesized with catalysts B, C, and D. Purified samples were also studied with this technique. XRD patterns for CNTs B after reaction and after purification are presented in Fig. 8. A crystalline phase of synthetic α-quartz, SiO_2, was found in the sample after reaction. No carbon or iron signals were observed. After purification, a diffractogram with the main peak at 25.5°, corresponding to an interlayer distance (d value) of 0.347 nm, was observed. XRD profiles for CNTs synthesized with catalysts C and D are shown in Figs. 9

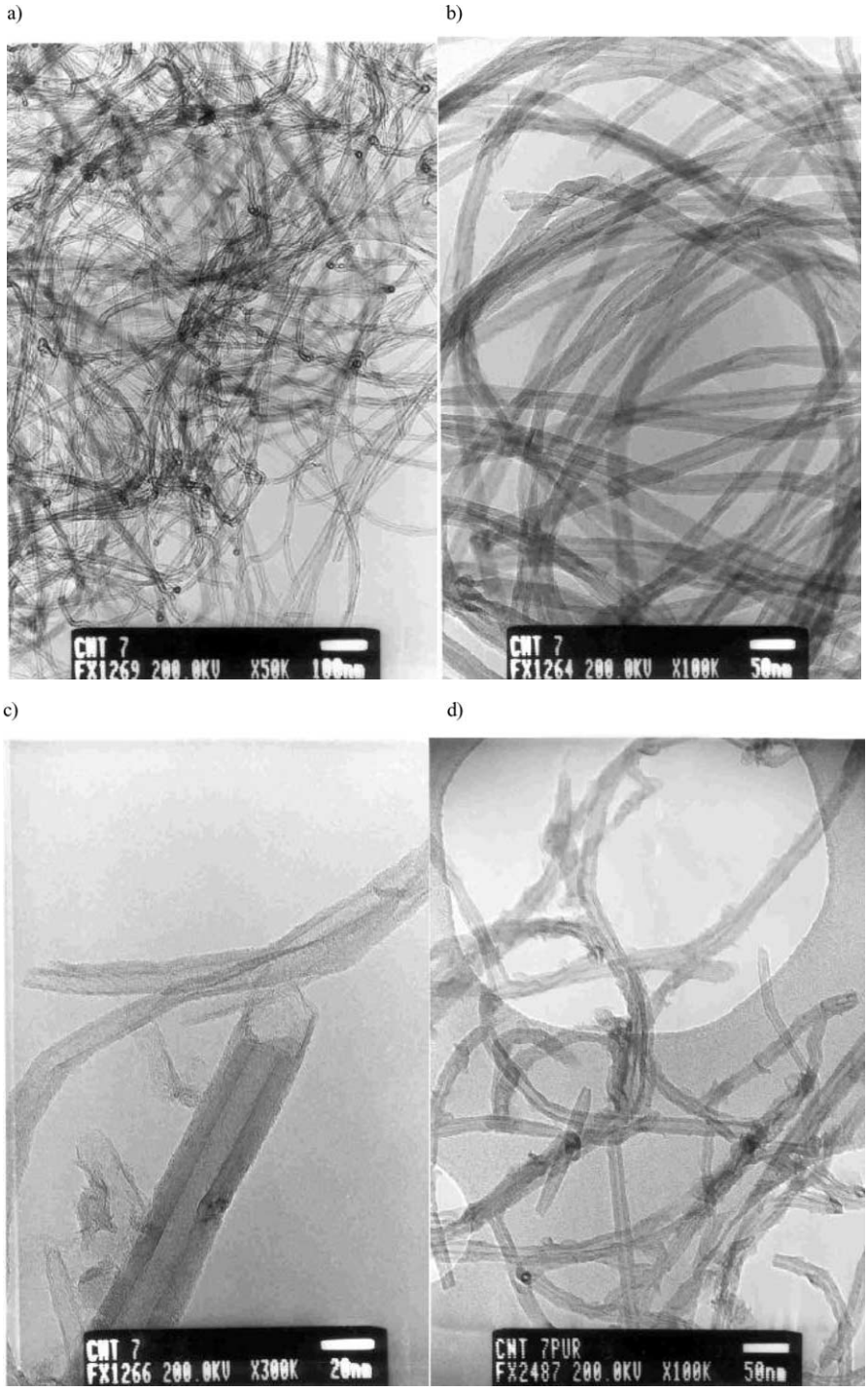

Fig. 6. TEM images of the products from reaction with catalyst C: (a, b) CNTs before purification treatments, (c) nanotube tip in detail showing amorphous carbon in the outer wall and defects in the structure, (d) CNTs purified and showing large amounts of amorphous carbon.

and 10, respectively. In Fig. 9 it can be seen that carbon structures are rather amorphous as revealed by the broad peak at 2θ values near 23°. However, in the purified sample (Fig. 9b) we can also identify a peak at 25.5° that we assume to be related to the presence of CNTs. Fig. 10 shows a crystalline phase of Fe_2SiO_4 and one small signal of α-Fe in sample D after reaction. No carbon signals were observed. After purification an intense signal from carbon at 26.4°, d value of 0.337 nm, and a crystalline phase of *syn*-cohenite, Fe_3C, between 40 and 50°, were observed. Table 4 summarizes the results obtained from the XRD study.

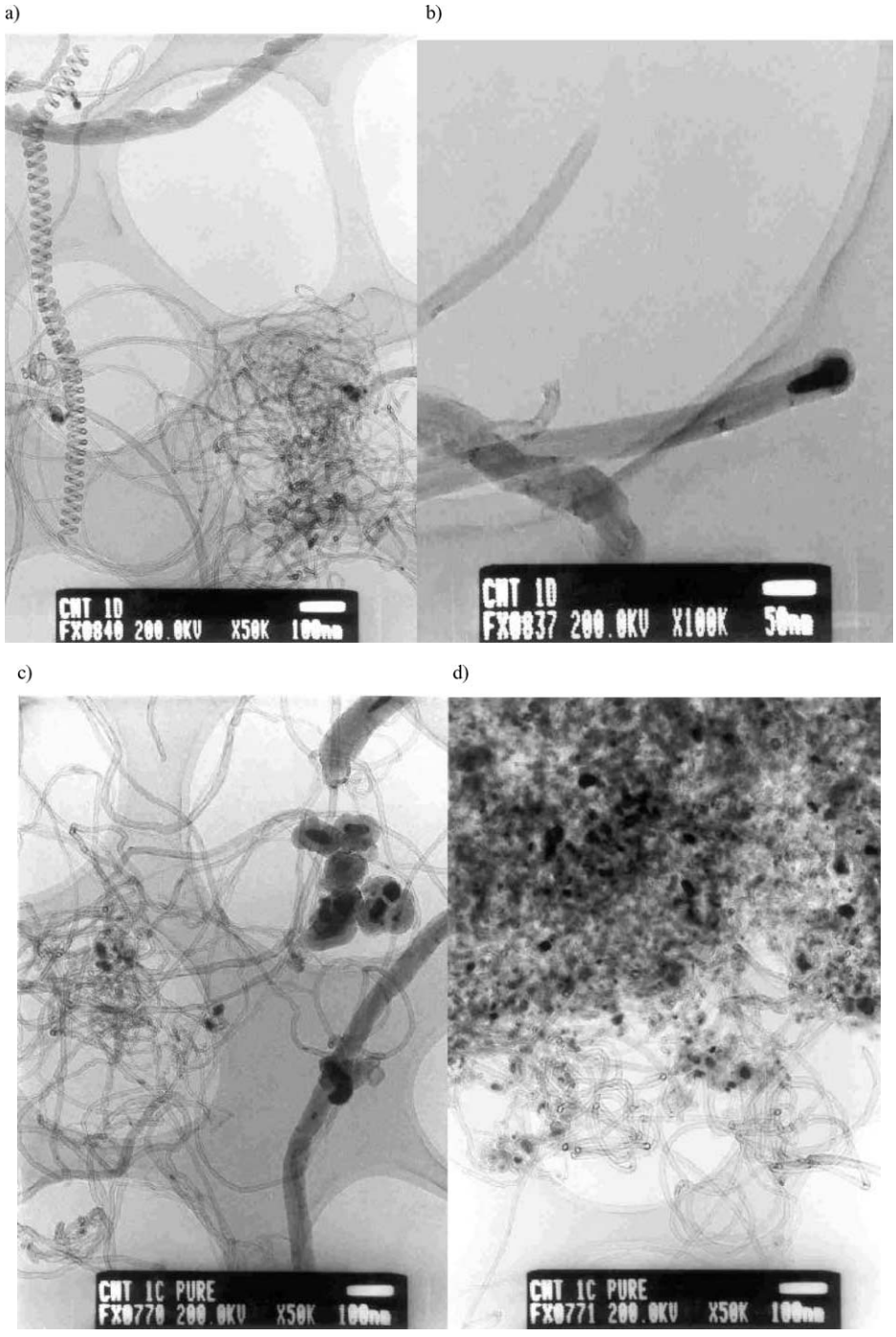

Fig. 7. TEM images of the products from reaction with catalyst D: (a) CNTs before purification, coiled structures, and CNFs, (b) metal particle in a nanotube tip, (c) sample after purification showing encapsulated carbon, CNFs, and CNTs, (d) CNTs after purification containing large amounts of metal (dark spots).

4. Discussion

Catalysts were prepared by the sol–gel method. Metal particle size and dispersion in the catalysts were reported to be decisive parameters in the synthesis of CNTs [8]. The sol–gel synthesis method ensures a highly homogeneous distribution of transition metal ions in the silica matrix. Improvement of the metal dispersion of the catalysts, to control the selective growth of well-defined CNTs, was the main objective of this work. The synthesis of these catalysts by the sol–gel method is highly influenced by different parameters, e.g., drying conditions, which should be controlled to make reproducible synthesis. In this work it was found, in agreement with previous results [20], that the higher iron contents yielded higher surface areas (Table 1) in the prepared samples. Determinations of the exact amount

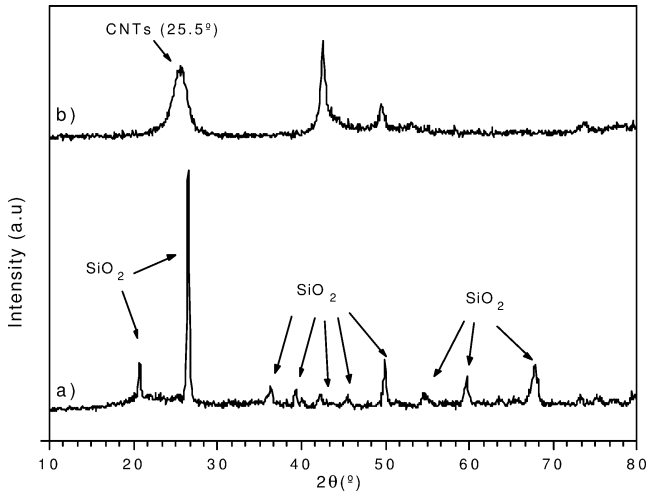

Fig. 8. XRD plots of products from reaction with catalyst B (a) after reaction and (b) after purification.

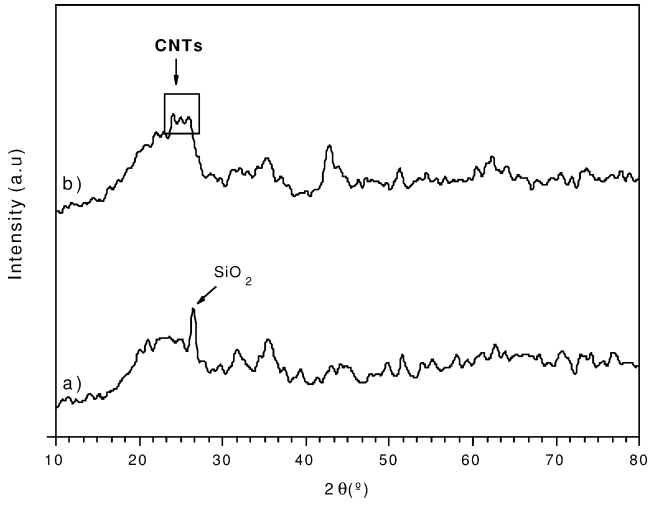

Fig. 9. XRD plots of products from reaction with catalyst C (a) after reaction and (b) after purification.

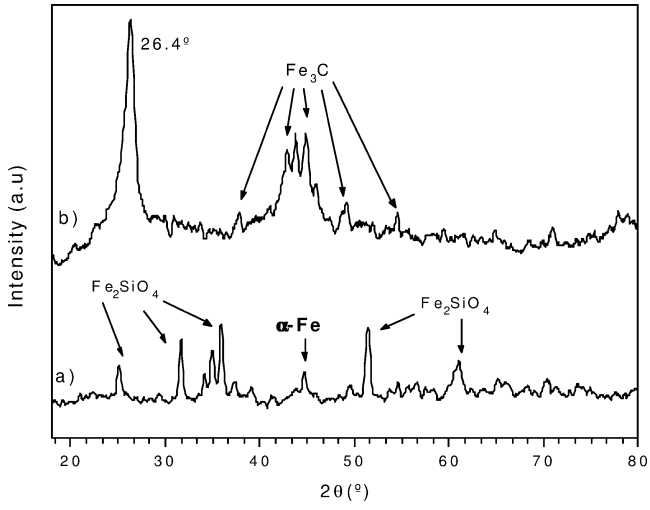

Fig. 10. XRD plots of products from reaction with catalyst D (a) after reaction and (b) after purification.

Table 4
XRD patterns of samples obtained from catalysts B, C, and D, before and after purification

Catalyst	XRD CNTs	XRD CNTs purified[a]	*d* value (nm)
B	SiO_2	CNTs (96%)	0.347
C	SiO_2	CNTs (87%)	–
D	Fe_2SiO_4	C (91%) + Fe_3C	0.337

[a] In parentheses is the carbon purity as determined from TPO experiments.

of metal at the surface and estimation of particle sizes, once the catalyst is submitted to a reduction treatment, are other limitations of this preparation method.

The TPR experiments gave evidence of the incomplete iron reduction in the catalysts after H_2 treatments at 723 K for 2 h. We have assumed that the iron atoms, on reduction, aggregate into metallic particles on the surface of the silica (iron–silica) matrix. The concentration of metallic iron at the surface of the catalysts has been calculated from the TPR data. It can be seen that, with the exception of sample A, the percentage of reduced iron decreases with increasing iron content of the sample (Table 2).

CO chemisorption was studied on catalysts previously reduced in H_2 at 723 K. Quantitative analyses of the CO chemisorption isotherms showed that an increment in the iron content resulted in lower chemisorption capacity. From the CO uptakes the metallic iron particle sizes in the catalysts were determined (Table 2). However, the average iron particle size, d, obtained from TPR data and CO chemisorption isotherms is not consistent with XRD observations. We assume that the catalysts are not strongly modified on increasing the temperature to 973 K in an inert atmosphere during reaction. In this way, we made a complete characterization after reduction treatments at this temperature. As was stated before, the metal particle size data in Table 2 provide an orientation about the metallic iron originated, and maybe not real values under reaction conditions.

XRD patterns for reduced catalysts A, B, and C showed noncrystalline phases for iron (not showed). This fact indicates that metallic iron is highly dispersed on the surfaces of these catalysts. However, an intense signal for α-Fe was clearly observed in catalyst D, showing the presence of large iron particles on the surface of this catalyst. A magnetite phase was also observed by XRD in this catalyst. Probably metallic iron underwent reoxidation during exposure to air at room temperature before the XRD analyses were carried out. Therefore, catalyst D showed large iron crystal sizes as detected by XRD in agreement with its low CO adsorption, as can be seen in the isotherm described in Fig. 2 and Table 2. The differences observed in determination of iron particle size from CO chemisorption experiments and XRD analyses can be explained by admitting that the segregated metallic iron particles are closely interacting with the sol–gel material. This interaction would lead to the occurrence of electron-deficient metallic iron particles with a hindered CO adsorp-

tion ability. That could be the reason why CO chemisorption was low for catalysts A, B and C, showing apparently large iron particle sizes but, however, nondetectable in XRD.

From the characterization data, it can be deduced that the degree to which the metallic iron is dispersed on the iron–silica matrix on reduction treatment is a function of the iron content of the iron–silica sample. By optimization of this parameter it is expected that a maximum number of active points for acetylene decomposition can be achieved and a correlation of the structure of the generated CNTs with these metal particle sizes established.

The synthesis of CNTs by chemical vapor deposition runs by a not well-defined mechanism. It is mostly assumed to involve adsorption and decomposition of the carbon source on the active points of the catalyst, formation of metal–carbon intermediate species, and finally growth of CNTs. In our reaction acetylene was supposed to be chemisorbed over the reduced iron particles exposed on the reduced catalyst surface. Second, an intermediate compound of Fe and C should be formed and finally CNTs should grow over the catalysts [23–27]. This mechanism supports the great importance of metal particle size in the catalyst. By controlling this parameter it would be possible to control the selective formation of CNTs and their structure (diameter, shape, texture, etc.).

Here we report that acetylene decomposition over the catalysts, prepared by the sol–gel method, leads to selectivities for CNT formation that vary with the metallic iron content and dispersion. TPO analyses after reaction revealed that the total amount of carbon deposited was clearly a function of the iron content of the catalyst, but these yields do not favor larger amounts of CNTs. Catalyst A is almost completely inactive for the carbon deposit production (0.1 wt%) and TEM images showed very scarce CNT formation. Catalyst B showed low carbon deposits after reaction ($\sim$ 1.75 wt% in carbon) and TEM images revealed high homogeneity in this raw material, showing mostly very clean and homogeneous CNTs of 8-nm internal diameter and 13-nm external diameter. Catalyst C was more active for acetylene decomposition ($\sim$ 4.10 wt% in carbon), but the quality of the CNTs obtained was lower that the quality of those obtained with catalyst B. Thus, nanotube wall deformations, amorphous carbon deposits on the outer walls, and formation of larger amounts of amorphous carbon were observed in sample C. Catalyst D showed the highest activity in acetylene decomposition ($\sim$ 10 wt% in carbon final deposit), but nonhomogeneity of the carbon products was observed in TEM images. In this case many species such as CNFs and amorphous carbon were found. It was also observed that iron particles were kept in CNT tips and carbon capsules (also revealed by XEDS analyses). Therefore, when metallic iron particles increase in size, the formation of nonselective forms of carbon (CNFs, amorphous carbon, etc.) is favored. In general the CNTs obtained were MWNTs, even though high-resolution TEM (HRTEM) analyses would be desirable to quantify the number of walls in all cases.

At this point it was of main importance to develop one method to quantify the products in exact percentages of CNTs over the total amount of carbon deposited after reaction. Several techniques have been used by many groups to achieve this quantification, but due to the similar graphite-like structure of CNTs and CNFs, it is quite difficult to determine. In this way TEM is the most reliable technique for characterizing CNTs, but only qualitatively. Resasco et al. carried out syntheses of CNTs by CO catalytic decomposition over several Co:Mo catalysts [35,36]. Quantification of the products was carried out by standard TPO. Although the metal present in the samples catalyzes their combustion, shifting the TPO peaks to lower temperatures, quantification and exact determination of the species observed were still possible in this case by using known references. Temperatures around 603 K were assigned to the combustion of amorphous carbonaceous deposits, around 783 K to SWNTs, and around 883 K to MWNTs. CNFs were supposed to burn off at lower temperatures than SWNTs. Based on the combustion temperatures of their nonpurified samples, a quantitative determination of the different carbon materials was established [36].

We have studied by TPO our purified samples, but the presence of different amounts of metal in these samples should cause modifications of the combustion temperatures. Thus, despite the high purity in CNTs, shown by sample B in TEM images, its combustion temperature was around 853 K due to a metallic residue content close to 4%. For sample C, similar behavior was detected. The highest carbon deposits are produced on catalyst D but TEM analyses revealed a lot of metal particles encapsulated in the carbonaceous structures, even after purification. The TPO final iron residue of this purified sample D was close to 10%. The presence of the metal can explain the low combustion temperature of this sample after purification. Two mass losses were observed for this sample, at 723 and 853 K. This could indicate the clear difference in combustion temperatures between nongraphitic structures, which burn at lower temperature, and graphitic structures such as CNTs and CNFs, which burn at higher temperature. However, the catalytic effect of the metal residue can distort this interpretation. The commercial CNTs displayed high combustion temperatures, so complete graphitization of these structures can be assumed. TPO profiles of the synthesized samples showed that their combustion temperatures were in all cases lower than those of the commercial CNTs. Therefore, it could be assumed that the former were not well-graphitized. In principle, TEM images corroborated the presence of some defects in the structure of CNT walls and significant amounts of amorphous carbon deposited on the outer walls of the tubes of catalysts C and D. However, the simultaneous presence of iron particles in the samples makes it impossible to attribute the lower combustion temperatures of our CNTs directly to as incomplete graphitization. An alternative explanation can be suggested to account for our TPO results. This is based on the assumption that the combustion temperatures of SWNTs,

MWNTs, and CNFs should be close to each other because of to their graphite-like structure. Therefore the temperature differences observed, among the different TPO profiles, could be caused not only by the various structures and degrees of graphitization of the carbon present in the samples, but also by the distinct amounts and dispersions of residual metal particles still present in the purified samples. It is known that the specific activity of metal catalysts for combustion reaction is a function of the surface exposed active centers.

Reduced sol–gel samples after reaction were submitted to XRD analyses with the exception of catalyst A, which was practically inactive. Evolution of the reduced sol–gel samples and evidence of types of carbon species formed in the reaction were obtained. Catalyst B showed amorphous phases before reaction. After ward, a crystalline phase of silica was observed. Neither iron nor carbon signals were observed, maybe because of the small amount of deposited carbon originally on this catalyst. After purification only carbon signals appeared in the XRD plot of catalyst B, with a d value of 0.347 nm. CNTs give an interlayer space higher than graphite (0.335 nm) because of their curved structure [37]. Then, the d value observed can be assigned to the presence of pure CNTs, as TEM images previously revealed. A similar picture can be described for the reaction products of catalyst C. Catalyst D evolved from iron oxide to α-Fe and Fe_3O_4 during reduction (Fig. 1), while after reaction (Fig. 10) Fe_2SiO_4 was identified [38]. These facts reveal incomplete reduction of iron during reaction, as TPR experiments indicated previously, and show that iron silicate can be assigned to the internal matrix of the sol–gel material. This iron silicate appeared better crystallized after reaction at high temperature (973 K). After purification of the carbon deposits obtained on catalyst D, no silica was observed, and only an intense carbon signal and iron carbide were detected (Fig. 10). The d value determined from this diffractogram was 0.337 nm for the carbon species present. This value is closer to that displayed by graphite structures (CNFs and capsules of carbon) than to that of CNTs. This interpretation is also supported by the TEM observations, where CNFs and capsules of carbon were present in high proportion. On the other hand, the iron carbide detected in Fig. 10 was attributed to the iron kept in CNT tips and capsules. At this point it can be speculated that this iron carbide could be related to CNT formation in agreement with the proposed mechanism for CNT growth [27], where this type of intermediate species has to be produced. Surface iron atoms reacting for CNT growth gave this intermediate species, meanwhile the excess of iron in catalyst D could just form the silicate, possibly helped by the incomplete reduction during reaction. Small iron particles should favor CNT growth and large iron particles should also form the iron carbide intermediate species, but non-CNT formation would be favored. That is why many other species were observed (CNFs, capsules of carbon, etc.) in samples prepared on catalyst D.

5. Conclusions

We have shown how the iron content of our catalysts can determine the final characteristics of the carbon deposits isolated after acetylene decomposition in a fluidized bed reactor at 973 K. Catalysts become more active in acetylene decomposition at higher iron contents, but this activity results in lower selectivity to homogeneous and well-defined CNTs, yielding high proportion of CNFs, capsules of carbon, and amorphous carbon. These results show the great importance of metal particle size in catalysts, and so, the mechanism proposed since the 1970s by Baker is supported [23]. Because this article demonstrated the presence of iron carbides during the catalytic synthesis of carbon nanotubes, it seems possible to admit the proposed mechanism, where an intermediate carbide compound is the key to explain the diffusion of the deposited carbon in the surface of the metal particle through the bulk of the metal.

Quantification of the exact amounts of the different carbon species obtained is difficult because of their similar properties. A proper method has not yet been developed to achieve this quantification in good agreement with qualitative microscopy observations. Much work is still needed to achieve high homogeneity and complete purification of the final carbon products synthesized.

Acknowledgments

This work has been supported by the *Foundation "Domingo Martínez"* and by the *Science and Technology Ministry Cabinet* (CICYT) in Spain (Grant MAT1999-1005 and MAT2000-0043-P4-03). We are also grateful to the *Microscopy Centre "Luis Bru,"* located in the Complutense University (UCM), Madrid, for TEM analysis. M.P.C. thanks the MECyD for a scholarship grant.

References

[1] P.M. Ajayan, Chem. Rev. 99 (1999) 1797.
[2] H. Dai, Surf. Sci. 500 (2002) 218.
[3] K.P. De Jong, J.W. Geus, Catal. Rev. Sci. Eng. 42 (2000) 481.
[4] W.K. Maser, A.M. Benito, M.T. Martínez, Carbon 40 (2002) 1685.
[5] T.W. Ebbesen, P.M. Ajayan, Nature 358 (1992) 220.
[6] T. Guo, P. Nikolaev, A. Then, D.T. Colbert, R.E. Smalley, Chem. Phys. Lett. 243 (1995) 49.
[7] S. Amelinckx, X.B. Zhang, D. Bernaerts, X.F. Zhang, V. Joanov, J.B. Nagy, Science 265 (1994) 635.
[8] M. Yudasaka, R. Kikuchi, Y. Ohki, E. Ota, S. Yoshimura, Appl. Phys. Lett. 70 (1997) 1817.
[9] Z.W. Pan, S.S. Xie, B.C. Chang, L.F. Sun, W.Y. Zhou, G. Wang, Chem. Phys. Lett. 299 (1997) 97.
[10] K. Hernadi, A. Fonseca, J.B. Nagy, D. Bernaerts, A.A. Lucas, Carbon 34 (1996) 1249.
[11] B.C. Liu, L.Z. Gao, Q. Liang, S.H. Tang, M.Z. Qu, Z.L. Yu, Catal. Lett. 71 (2001) 225.
[12] D. Venegoni, Ph. Serp, R. Feurer, Y. Kihn, C. Vahlas, Ph. Kalck, Carbon 40 (2002) 1799.
[13] K. Hernadi, A. Fonseca, J.B. Nagy, A. Siska, I. Kiricsi, Appl. Catal. A 199 (2000) 245.

[14] J. Kong, A.M. Cassele, H. Dai, Chem. Phys. Lett. 292 (1998) 567.
[15] P. Serp, A. Madroñero, J.L. Figueiredo, Fuel 78 (1999) 837.
[16] A. Maroto-Valiente, P. Navarro-López, I. Rodríguez-Ramos, A. Guerrero-Ruíz, C. Li, Q. Xin, Carbon 38 (2000) 2003.
[17] M.A. Ermakova, D.Y. Ermakov, A.L. Chuvilin, G.G. Kuvshinov, J. Catal. 201 (2001) 183.
[18] Ph. Mauron, Ch. Emmenegger, A. Züttel, Ch. Nützenadel, P. Sudan, L. Schlapbach, Carbon 40 (2002) 1685.
[19] T. Ida, H. Tsuiki, A. Ueno, K. Tohji, Y. Udagawa, J. Catal. 106 (1987) 428.
[20] D. Li, D. Wu, X. Wang, L. Lu, X. Yang, Mater. Res. Bull. 36 (2001) 2437.
[21] Á. Kukovecz, Z. Kónya, N. Nagaraju, I. Willems, A. Tamási, A. Fonseca, J.B. Nagy, I. Kiricsi, Phys. Chem. Chem. Phys. 2 (2000) 3071.
[22] V.N. Parmon, G.G. Kuvshinov, V.A. Sadykov, V.A. Sobyanin, Stud. Surf. Sci. Catal. 119 (1998) 677.
[23] R.T.K. Baker, P.S. Harris, R.B. Thomas, R.J. Waite, J. Catal. 30 (1973) 86.
[24] A.J.H.M. Kock, P.K. de Bokx, E. Boellaard, W. Klop, J.W. Geus, J. Catal. 96 (1985) 468.
[25] J.W. Snoeck, G.F. Froment, M. Fowles, J. Catal. 169 (1997) 240.
[26] S.H. Lee, E. Ruckenstein, J. Catal. 107 (1987) 23.
[27] A. Sacco Jr., P. Thacker, T.N. Chang, A.T.S. Chiang, J. Catal. 85 (1984) 224.
[28] P. Navarro-López, I. Rodríguez-Ramos, A. Guerrero-Ruíz, in: J.M. Órfão, J.L. Faria, J.L. Figueiredo (Eds.), Actas do XVII Simpósio Ibero-Americano de Catálise, Porto (Portugal), 2000, p. 87.
[29] P. Navarro-López, I. Rodríguez-Ramos, A. Guerrero-Ruíz, in preparation.
[30] J. Santamaría, J. Herguido, M.A. Menéndez, A. Monzón, in: J. Santamaría, J. Herguido, M.A. Menéndez, A. Monzó (Eds.), Ingeniería de Reactores, Síntesis, Madrid, 2002, p. 207.
[31] I. Fernández-Morales, A. Guerrero-Ruíz, F.J. López-Garzón, I. Rodríguez-Ramos, C. Moreno-Castilla, Carbon 22 (1984) 301.
[32] P. Möller, H. Papp, Adsorpt. Sci. Technol. 4 (1987) 176.
[33] A. Guerrero-Ruíz, PhD thesis, Universidad de Granada, 1983.
[34] J.R. Anderson, Academic Press, New York, 1975, p. 295.
[35] B. Kitiyanan, W.E. Alvarez, J.H. Harwell, D.E. Resasco, Chem. Phys. Lett. 317 (2000) 497.
[36] W.E. Alvarez, B. Kitiyanan, A. Borgna, D.E. Resasco, Carbon 39 (2001) 547.
[37] L. Ci, B. Wei, C. Xu, J. Liang, D. Wu, S. Xie, W. Zhou, Y. Li, Z. Liu, D. Tang, J. Cryst. Growth 233 (2001) 823.
[38] J.I. Sohn, C.J. Choi, L. Lee, T.Y. Seong, Appl. Phys. Lett. 78 (2001) 3130.